SARS-CoV-2: Theoretical analysis of the proposed algorithms to the Enhancement and Segmentation of High-Resolution Microscopy Images. Part II

Roberto Rodríguez (rrm@icimaf.cu)
ICIMAF
Brian A. Mondeja
CEA
Odalys Valdes
IPK
Sonia Resik
IPK
Ananayla Vizcaino
CEA
Emilio F. Acosta
CEA
Yorexis González
CEA
Vivian Kourí
IPK
Angelina Díaz
CEA
María G. Guzmán
IPK

Research Article

Keywords: Theoretical analysis, Image enhancement, Segmentation, Algorithms, Coronavirus SARS-CoV-2, Microscopy

Posted Date: November 18th, 2020

DOI: https://doi.org/10.21203/rs.3.rs-109694/v1

Version of Record: A version of this preprint was published at Signal, Image and Video Processing on January 12th, 2022. See the published version at https://doi.org/10.1007/s11760-021-02045-7.

SARS-CoV-2: Theoretical analysis of the proposed algorithms to the Enhancement and Segmentation of High-Resolution Microscopy Images. Part II

Roberto Rodríguez[1]*, Brian A. Mondeja[2]; Odalys Valdes[3]; Sonia Resik[3]; Ananayla Vizcaino[2]; Emilio F. Acosta[2]; Yorexis González[2]; Vivian Kourí[3]; Angelina Díaz[2]; María G. Guzmán[3]

Abstract. Today is a reality that the novel coronavirus SARS-Cov-2 has become a global pandemic. For this reason, the study of real microscopic images of this coronavirus is of great importance, as it allows us to carry out a more precise research on it. However, as we pointed out in a former paper [1], many times these microscopic images present some blurring problems, which are always susceptible to be improved. The aim of this work is to carry out a theoretical analysis of the proposed algorithms to enhancement and segmentation of these microscopic images, which result important for the design and development of future algorithms before new epidemics.

Keywords. Theoretical analysis, Image enhancement, Segmentation, Algorithms, Coronavirus SARS-CoV-2, Microscopy

1. Introduction

Today is a reality that the virus SARS-Cov-2 has become a global pandemic. This novel virus, named coronavirus due to visual appearance -under electron microscopy- similar to a crown [2], it is the cause of an infectious disease by severe acute respiratory syndrome (SARS-Cov-2) [3], and named by the World Health Organization (WHO): *COVID-19*.

Image analysis is a scientific discipline providing theoretical foundations and methods for solving problems appearing in a range of areas as diverse as the pathology, biology, astronomy, medicine, physics, geography, chemistry, robotics, and other. Particularly, computer vision is an interdisciplinary field that deals with how computers can develop a high-level understanding by interpreting information present in digital images [4]. It has made substantial progress in the last few years, which might be of interest and importance, not only for image analysis but also, for example, within image segmentation and enhancement, for the development of digital models in the range-space domain [5].

The microscopic study of images of viruses and bacteria is very important and of great need, since it allows us to carry out a more precise and local research on them. However, many times these microscopic images present some blurring problems, which often makes it difficult to analyze correctly to them [1].

* Corresponding author: Roberto Rodríguez
rrm@icimaf.cu

[1] Institute of Cybernetics, Mathematics, and Physics of Cuba (ICIMAF)

[2] Center for Advanced Studies of Cuba (CEA)

[3] Institute of Tropical Medicine ¨Pedro Kourí ¨ (IPK)

The obtaining high-quality microscopic images is not always a trivial process, even in the best microscopes, due to physical phenomena that originate between the glass coverslip, light and microscope optics. Some of these phenomenons are, scattering, out-of-focus, imperceptible vibrations, voltage disturbances, among others, which causes certain blurring in the microscopic images [1].

In order to improve such problems is necessary to design and develop algorithms that take into account the physics of formation of those microscopic images, as the correlation between pixels, boundary conditions, among others. For this reason, one focuses the greatest attention on the algorithmic part in order to find a solution to the physical phenomena mentioned above, which are the causes of blurring in microscopic images. However, many times around these algorithms lies a theoretical basis that is worth analyzing, since it can help to face new problems of similar magnitudes.

The aim of this work is to carry out a theoretical analysis of the proposed algorithms to the enhancement and segmentation of SARS-Cov-2 high-resolution microscopy images, where in [1]; we addressed the most attention to the application of those algorithms.

The rest of paper is organized as follows: in Section II, the materials, methods and the characteristics of studied images are given. Section III outlines the *Algorithms* and related theoretical aspects. Section IV contains the experimental results and discussion. We describe our conclusions in Section V.

2. Materials and methods

As we expressed in [1], we captured microscopic images from nasopharyngeal swabs collected from Cuban individuals with *COVID-19* symptomatic and RT-PCR positive for SARS-CoV-2, and processed by Scanning Electron Microscopy, Confocal Microscopy and, Atomic Force Microscopy [6]. We completed a database of more than 1010 microscopic images.

In the case of SARS-CoV-2, the Scanning Electron Microscopy (SEM) images provide fundamental data of the structural aspects of the virus [1], [6], which can be a guiding point to design and development of algorithms and analysis of associated theory.

2.2. Characteristics of studied images

In this section, we will carry out a more detailed analysis of the characteristics of study images with aim that one can better

understand the proposed algorithm in [1], some variants of it, and its corresponding theoretical analysis.

In Figure 1, we show two examples of typical coronavirus images. One can see other examples, captured via SEM, in [1].

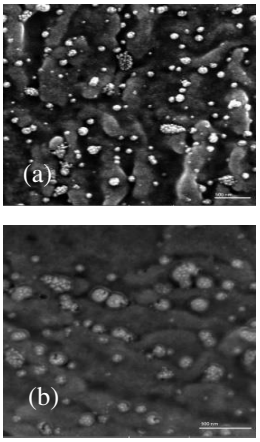

Fig 1. Characteristic of coronavirus microscopic images. (a) and (b), original microscopic images.

In Figure 1, (a) and (b), one can observe several notable characteristics of these microscopic images of the novel coronavirus, the most notable being its appearance of blurring, which it is typical in images captured via SEM. Here, the important issue is to be able to improve and isolate the *S-spikes*.

It is known that scientists have given the name coronavirus by the crown of *S-proteins (*also called *S-spikes)* covering their outer membrane surface. And many works have focused on these *S-proteins*, because they are the keys that the virus uses to enter host cells; where these *S-proteins* bind to a receptor called angiotensin converting enzyme 2 (ACE2) to hack its way into host cells. [7].

In addition, studies so far suggest that the *S-proteins* of the novel coronavirus bind to ACE2 significantly more strongly than those of SARS-CoV, and probably that is one of the reasons it spreads more easily and is more infectious [7].

Everything expressed denotes the importance of enhancing and isolating the *S-proteins* in the blurring microscopic images of the new coronavirus.

In [1], we presented a set of typical characteristics of microscopic images of the novel coronavirus. However, one can note in Figure 1 that the *S-proteins* of the virus are hyper-dense regions (clearer areas), this being one of the most notable features of these microscopic images. We used this caracteristic to design the algorithm we proposed in [1]. In this work, one will see variants of that strategy, and a deeper theoretical analysis.

3. Algorithms and related theoretical aspects

We will address in greater depth the theoretical aspects related to the proposed algorithms for the enhancement and isolation of *S-proteins*.

In Figure (1), it is important to observe that the *S-spikes* are clearer small dots than its surrounding background, grouped in areas corresponding to the virus and scattered throughout the image. Then, within a region of microphotographs, changes in intensity levels can effectively distinguish *S-spikes*, which is indicative that the correlation between pixels, corresponding to the *S-proteins*, in those areas is stronger than outside them. Therefore, this analysis indicates that one must work in the region of interest (RoI), locally and using small masks (*3x3* or *5x5* dimension) to carry out the processing [8].

3.1 Some definitions

A. Filtering process

Most of time, medical images are corrupted with lot of noise, due to phenomena that occur in the A/D converter (and often called white noise), which produce attenuation of high spatial frequencies (edges, corners, points, etc.), and which makes it difficult to carry out a better interpretation of the scene. This phenomenon also occurs in the microscopic images.

This type of noise (information of high spatial frequencies) is overlapped to important aspects in images, being necessary, for its attenuation, to use alternative strategies. The main problem in the reduction of noise is to get a clean image; that is, without noise, but keeping all attributes of the original scene as could be the shape, size, color, edges, among others.

Many methods have been proposed so far for the elimination of white noise, among them, the "*had hoc*" filters, the mean and Gaussian filters [9], and more recently, the *Mean-Shift Iterative Algorithm* (*MSHi*) [8], which is more adaptive, but it consumes more computational time. For that reason, we used the Gaussian filter with good results, which by the shape of this function attenuates the noise more strongly in the central part, and edges are less smoothed.

We carried out several researches with many microscopic images, arriving to the conclusion that the best performance are obtained, according to our application, with $\sigma = 3$. We verified that for large values of sigma ($\sigma > 4$) the smoothing was poor, because homogeneous areas arose in the filtered image and some of *S-proteins* were joined. This was the reason why we decided to carry out our experiments with the parameter equal to *3*. The used window size was of *3x3* too. We verified that with this window size, we considerably smoothed the noise and did not affected the edges of interest objects (the *S-spikes*). This is because the *proteins-S* have a smaller size in relation to its environment (see Fig. 1).

B. About the mathematical morphology

Definition 1: *(Morphological opening)*

Morphological opening is the dilation of the erosion of a set $\boldsymbol{I}$ by a structuring element $\boldsymbol{S}$, that is,

$$Opening = I \circ S = (I \ominus S) \oplus S, \quad (1)$$

where, the symbols $\ominus$ and $\oplus$ denote erosion and dilation, respectively.

Morphological opening removes small objects from the foreground of an image (usually taken as the bright pixels: edges, corners, points, etc.). If one uses a large structuring element, one can obtain the background of image. Many times, opening operates similar to a low pass filter.

Definition 2: *(Decomposition at thresholds)*

Let $T_h(I)$ be the successive thresholds of I, for $h = 0$ to $L-1$,

$$T_h(I) = \{ p \in D_I \,/\, I(p) \leq h \} \quad (2)$$

Then, they constitute the threshold decomposition of I, and these sets satisfy the following inclusion relationship [5]:

$$T_h(I) \subseteq T_{h-1}(I) \qquad \forall\ h \in [0, L-1], \quad (3)$$

where, I is an image of gray levels, D_I is the domain of I and L is the number of gray levels.

Definition 3: *(Regional maximum).* A regional maximum at altitude h of greyscale image I is a connected component C of $T_h(I)$ such that $C \cap T_{h+1}(f) = \varphi$,
where, the symbol φ means the empty set.

One should not confuse a regional maximum with a local maximum. A pixel ***p*** of I is a local maximum in an h environment, if and only if, the $I(p)$ value is greater than or equal to any of the pixels in your environment. However, a regional maximum is a set of pixels connected at an h height where there is no pixel with a value higher than that height. Therefore, we can consider each of the *S-spikes* as local and non-regional maxima. One should have this concept clear since, in this application, is very important for the design of algorithms.

Definition 4: *(Grayscale reconstruction).* The grayscale reconstruction $\rho_I(J)$ of I from J obtained by iterating grayscale dilations of J "under" I until stability is reached, that is,

$$\rho_I(J) = \bigvee_{n \geq 1} \delta_I^{(n)}(J) \quad (4)$$

Reconstruction is an efficient method for extracting regional maxima and minima in gray level images.

However, we did not follow this path in the design of our algorithms, because in the initial tests carried out, we did not obtain good results. Reconstruction produced a connection of the *S-spikes*, which is not convenient in this application. One can find the explanation of this in what we expressed in previous paragraphs (the *S-spikes* are local maxima, non-regional).

Definition 5: The *h-dome* transformation ($D_h(I)$) of the *h-domes* of a greyscale image ***I,*** it is given by,

$$D_h(I) = I - \rho_I(I - h) \quad (5)$$

The *h-dome* transformation extracts light structures without involving any size or shape criterion. The only parameter *(h)* related to the height of these structures. In the case of coronavirus *S-spikes* isolation, this parameter was of vital importance.

The need to be able to isolate the *S-proteins* individually has great importance because it will allow establishing a surface density index, where at higher index, the higher the virulence level.

C. About enhancement and segmentation of images

Definition 6: (*Extreme filter).* The *Extreme filter* is defined by the following expression,

$$g = E_{ext}(I) = \begin{cases} max(I) & if\ \ max(I) - I \leq I - min(I) \\ min(I) & otherwise \end{cases}, \quad (6)$$

where, *max (I)* is the maximum value of pixel in the window, and *min (I)* is the minimum value of pixel.

The extreme filter has been widely used to accentuate blurring sides and step sides in biological images. This one is very useful when one combines it with other filters, and its behavior is similar to a high pass filter. We used, due to small size of the *S-spikes*, window size of *3x3*. We utilized the extreme filter in the initial experiments, but we did not obtain good results in the isolation of the *S-proteins* (due to space problems, we did not present the results here). We concluded that these results were due to that edges of the *S-proteins* are insignificant (very little thickness) in relation to the morphology of coronavirus, and they are joined in the filtering process.

Definition 7*: (High spatial frequencies).* From a *Digital Image Processing* point of view, the spatial frequency is a measure of how often small details (points, edges, corners, steps, etc.) of a structure repeat per unit of distance (that is, any structure that is periodic or not across position in space).

In this research, we consider the *S-proteins* as information of high spatial frequencies. Therefore, we focused our goal on these frequencies; that is, we try to enhance their contrast or isolate them, but always processing locally.

A typical expression for local contrast enhancement is as follows,

$$g(x,y) = \mu + k\,(f(x,y) - \mu) \quad (7)$$

where, the symbol "μ" is the mean at a given window and k is a gain factor.

One can consider the expression (7) as the equation of a straight line, where there can be many variants of her. In addition, the second term is high-frequency information, a measure of local variability in the image, and one can consider to *"k"* as the slope [9].

In fact, if $k > 1$ the contours of image will be sharpened and its performance is similar to a high pass filter. If the parameter k is in the closed range, $0 \leq k \leq 1$, then the image will be smoothed similar to a low pass filter. In the extreme case, $k = 0$, the result will be equal to the local average. Many times, the first μ is replaced by $f(x, y)$, i.e., the original image.

An algorithm by using expression (7) can increase either sharpness or local contrast because these are both ways of increasing differences between values, since increasing slope, sharpness referring to very small-scale differences (high frequency), and contrast referring to larger-scale (low frequency).

For example, a variant of the expression (7) is to replace in the second term to μ by the Gaussian function. In this case, one should take small window size and small σ too, since for one to achieve good results the scale (σ) must be of similar dimension

to the structures that one want either to sharpen or to enhance (the *S-proteins*) [10].

What we expressed in the previous paragraph was the fundamental base of the final version of our algorithm, and always processing the image locally; otherwise, results will be bad [1]. In effect, the importance of locally processing the image, it is to take in consideration the spatial relation (and implicitly the correlation among the pixels). This makes that the performance of algorithms improve substantially [8].

3.2 Algorithms. Analysis

In any application of computer vision, the study and characterization of images are of vital importance. The correct design of algorithms and their good performance depend on the quality of this study.

In [1], we carried out a characterization of the microscopic images captured by Scanning Electron Microscopy, from nasopharyngeal swabs collected from Cuban individuals with COVID-19 symptomatic and RT-PCR positive for SARS-CoV-2.

In this section, we will expose and carry out an analysis of three designed algorithms, taking as base the study of the microscopic imagens and an appropriate combination of the theory described above.

An aspect to highlight in these strategies is their algorithmic simplicity. Today, to many of problems that arise in computer vision, researchers apply deep learning, which requires of big databases and has a computational cost too [11, 12, 13]. However, when one carries out a deep study of the images, one can obtain good results of fast way and with good performance of the algorithms, without the need of using complex methods.

Without doubt, deep learning has given very good results, especially in identification of patterns; but in this application one want either to sharpen or to enhance certain spatial frequencies (the *S-pikes*), which have a random spatial distribution of viruses in viruses.

Algorithm No.1

***Data**: Original image **A**, parameter (h);*
***Result**: Enhanced or sharpened image. Let **B** be*

1. *Initialize: **h = 60, window size = 3x3, sigma (σ) = 1.5,***
2. *Pass the Gaussian filter to the original image (Optional). Let **C** be the result*
3. *Subtract the **h** parameter from **C.** Let **D** be the result*
4. *Accentuate high spatial frequencies by using expression (7) with the Gaussian function. Let E be the result.*
5. *Apply an extreme filter according to expression (5). Let **B** be the result.*
6. *Return **B***

End;

Observe that only the subtraction of the *h* parameter we carry out it in a global way. In all the next steps, we work locally, and we process similar in how one treats the convolutional neural networks.

In effect, in the *Gaussian* and *Extreme* filters, we compute the spatial size of the output as a function of the input size, the stride with which they are applied, and the amount of zero padding used on the border [11]. In this case, due to the size of the *S-spikes*, we used a stride equal to one, since with this stride, we obtained more precision; that is, a bigger stride causes sharpness loss of *S-proteins*.

Algorithm No. 2

***Data**: Original image **A**;*
***Result**: Enhanced or sharpened image. Let **B** be*

1. *Select a structuring element type "Disk" with a large diameter Let **S** be*
2. *Background = Opening (**A**, **S**). Let **C** be the result*
3. *Subtract **C** from **A.** Let **D** be the result*
4. *On **D**, accentuate high spatial frequencies by using expression (7), with the Gaussian function and the same used parameters Let **B** be the result*
5. *Return **B***

End;

We proceeded with the *Algorithm No. 2* of very similar way as we did with the *Algorithm No. 1*.

However, it is interesting to point out that the value of the *h* parameter determines if to increase either sharpness or local contrast. For a small value of *h*, the *S-spikes* are enhanced (more contrasted) in relation to the original image. While, for a bigger value of *h*, the *S-spikes* are sharpened (practically segmented), where the *S-spikes* appear clear on a black background.

The importance of enhancing or segmenting the *S-spikes* is because those areas that showed a high density of the *S-spikes* and pseudohyphae projections appear to be related to an active zone of viral germination [6]. Therefore, being able to isolate the *S-proteins* will allow to establish an "*index*" that relate the number of the *S-proteins* per unit area (surface density), where at higher index, the higher degree of virulence.

Algorithm No. 3

***Data**: Original image **A**, parameter (h);*
***Result**: Enhanced or sharpened image. Let **B** be*

1. *Initialize: **h = 90, window size = 3x3, sigma (σ) = 2.0***
2. *Pass Gaussian filter to the original image (Optional). Let **C** be the result*
3. *Subtract the **h** parameter from **C.** Let **D** be the result*
4. *Accentuate high spatial frequencies by using expression (7) with the Gaussian function. Let E be the result.*
5. *Go to step 4 again. Let **B** be the result.*
6. *Return **B***

End;

See that *Algorithm No. 3* is simpler than the previous two strategies, and it was with which the best results were obtained.

4. Experimental results. Discussion

It is a reality that today; many computer vision researchers are increasingly using algorithms from Deep learning (DL) to help build robust and reusable vision systems. Just as learning is an essential component of biological visual systems, artificial systems that learn and adapt represent an important challenge in modern computer vision research.

Automated analysis of biomedical images remains a considerably challenging task mainly because biomedical images are complex and variant. Moreover, the SARS- CoV-2 pandemic has demonstrated that the difference between disease and non-disease cases is often subtle.

Therefore, accurate automated analysis of biomedical images requires the development of innovative strategies that are adaptive and scalable, which it is possible, with a deep study of the images to be processed that avoids the blind use of complex methods which consume computational time, and that in the end do not provide the expected results.

In Figures 4 and 5, we show some examples of the obtained results of applying the *Algorithm No.1* to some SARS-CoV-2 microscopic images for four values of *h* parameter.

In Figures 4 and 5, one can see the fundamental characteristic that present all original microscopic images: the blurring, which it was common to all samples captured by Scanning Electron Microscopy.

Note that the processed images of applying the *Algorithm No. 1* were notably enhanced; that is, contrast increased, and the *S-spikes* are more evident and shows the urchin-shape. One can observe that for small values of *h*, we obtained a better-contrasted image (*h=30*), while as the value of *h* increased (*h=100*), the *S-spikes* have more sharpness, where one can see white areas on a black background. This result permits to carry out an automatic analysis of the density of the *S-spikes* (number of *S-spikes*/ area unit); that is, automatic count of white points on a black background area, and one can establish an index.

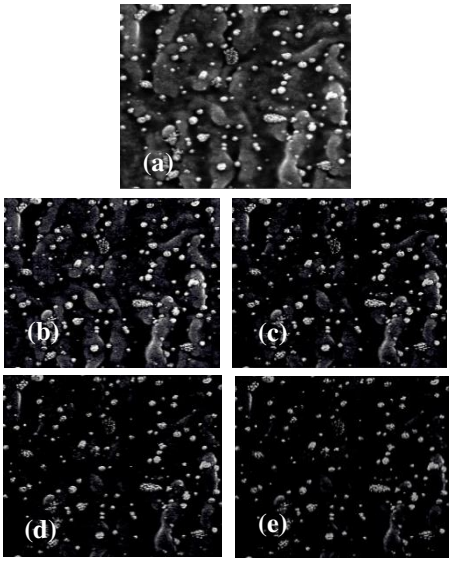

Fig. 4 Application of *Algorithm No. 1* for different values of *h* parameter. (a) Original image, (b) *h=30*, (c) *h=60*, (d) *h=80*, (e) *h=100*.

The advantage of the *Algorithm No.1* is that with a single parameter (the others: window sizes and sigma remain unchanged), one can increase either sharpness or local contrast. For an *h* parameter very large a practically segmented image can be reached.

Now, we will present the achieved results by using the *Algorithm No. 2*. In Figures 6 and 7, we show the obtained results, taking respectively as original images Figures 4 (a) and 5 (a).

In the *Algorithm No. 2*, the choice of a structuring element type *"Disk"* was due to the round morphology presented by the SARS-CoV-2 coronavirus. We verified that the radius size has a behavior contrary of the *h* parameter in the *Algorithm No. 1*, in the sense that for smaller radius size increases the sharpness (see Figs. 6(a) and 7(a)), while for larger size increases the local contrast (see Figs. 8(d) and 9(d)).

Visually comparing the performance of the *Algorithms No. 1* and *No. 2*, subjectively it appears that the *Algorithm No. 1* accentuates the high frequencies more, and therefore, produces a greater local contrast and greater sharpness in the *S-proteins*. With the *Algorithm No. 1*, the background looks darker

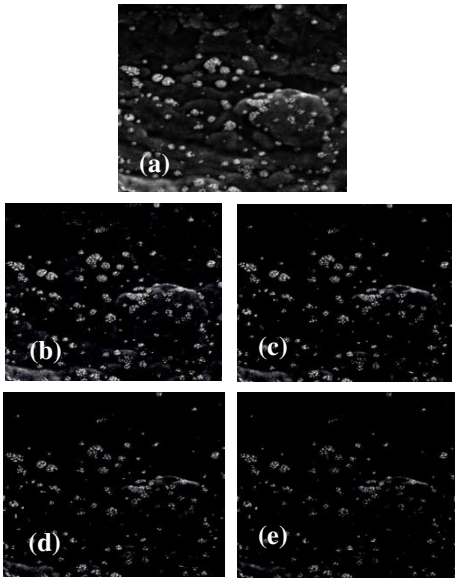

Fig. 5. Application of *Algorithm No. 1* for different values of *h* parameter. (a) Original image, (b) *h=30*, (c) *h=60*, (d) *h=80*, (e) *h=100*.

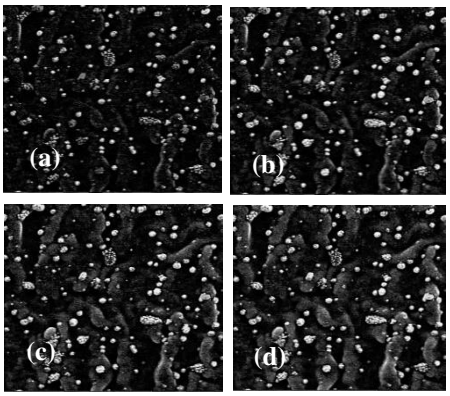

Fig. 6. Application of the *Algorithm No. 2* for a structuring element type "*Disk*" for different radios. Original image Fig. 4(a). (a) *Radio =15*, (b) *Radio = 25*, (c) *Radio = 35*, (d) *Radio = 45.*

The reality is that both algorithms were able to enhance the local contrast and sharpness of the *S-proteins.*

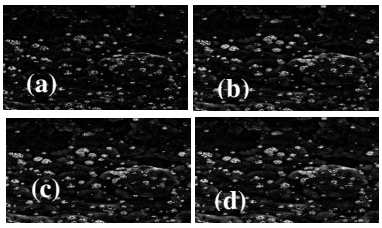

Fig. 7. Application of the *Algorithm No. 2* for a structuring element type "*Disk*" for different radios. Original image Fig. 5(a). (a) *Radio =15*, (b) *Radio = 25*, (c) *Radio = 35*, (d) *Radio = 45.*

Now, the obtained results with the *Algorithm No. 3*. Figures 8 and 9 show these results. The original images are the same.

In Figures 8 and 9, one can observe that the *Algorithm No. 3*, compared with the other two, produced the bigger local contrast and sharpness, and the *S-pikes* were notably highlighted. One can note, in this case, that for an *h* bigger than 80, the processed image is close to a segmented image (the *S-spikes* are saw as white points), and the background is practically zero. All contrary occurs for small *h*, where the *Algorithm No. 3* only enhanced the local contrast.

For example, in Figure 10, we represent the profiles with the processed images by using the *Algorithms No. 2* and *No. 3* for *R=15* and *R*=45, and *h = 30* and *h = 100* respectively. The horizontal profiles through images are a plot of the pixel intensities along a single row.

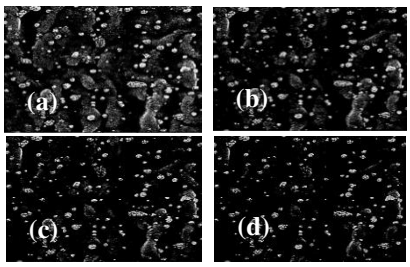

Fig. 8. Application of *Algorithm No. 3* for different values of *h* parameter. Original image Fig. 4(a). (a) *h=30*, (b) *h=60*, (c) *h=80*, (d) *h=100.*

One can see in Figures 10 and 11 that the peaks of the profiles, for an *h = 100* begins to flattening. In other words, parallel lines to the "***x***" axis on peaks are indicative of equal intensity levels (segmented zone). In addition, the peaks begin to separate, which shows the isolation of the *S-spikes* at different areas where the coronavirus are. The intensity of background reached zero value.

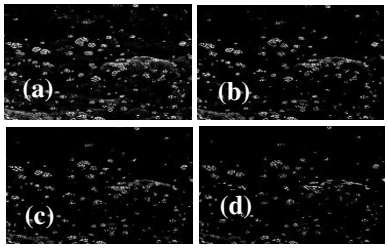

Fig. 9. Application of *Algorithm No. 3* for different values of *h* parameter. Original image Fig. 5(a). (a) *h=30*, (b) *h=60*, (c) *h=80*, (d) *h=100.*

In the case of the *Algorithm No. 2*, the slopes of profiles are smoother, that is, less abrupt, which means that this algorithm is fundamentally useful for local enhancement.

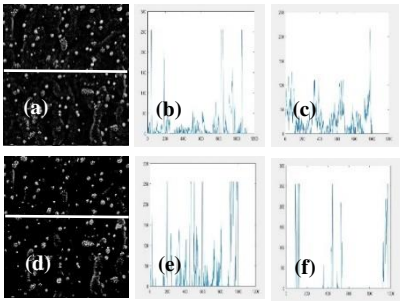

Fig. 10. Profiles with the processed images by using the *Algorithms No. 2* and *No. 3.* (a) Processed image and a profile, (b) *R=15*, (c) *R=45*, (d) Processed image and a profile, (e) *h = 30*, (f) *h = 100.*

When observing Figure 10, we can highlight that the slopes of the profile curves, when using the *Algorithm No. 3*, were more abrupt than those when using the *Algorithms No. 1* and *No. 2* (we, due to space problems, did not present those for the *Algorithm No. 1*).

It is important to note, that the proposed *Algorithms* are hybrid strategies, obtained by a combination of methods of the mathematical morphology and the statistical, but one always locally processing the images. On the other hand, one can observe the algorithmic simplicity of these strategies, with the use of very few adjustment parameters, which makes them more adaptable to real problems.

4.1 Comparisons with other methods. Quantitative evaluation

In this section, we will carry out a comparison of our three strategies with two recognized classical techniques, which will be used locally; in order to achieve bigger effective in the comparison. These classical techniques are a *high pass filter (HPF)* and a *statistical local contrast enhancement (SLCE)* [9]. However, such a comparison will always be incomplete given the information volume existing in the literature.

In Figures 11 and 12, we show the obtained results with the *HPF*, with the *SLCE* and with our algorithms. As original images, we used Figures 4(a) y 5(a).

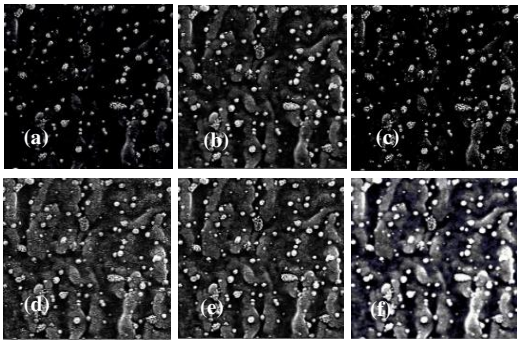

Fig. 11. Comparisons with two classical methods. Original image Fig. 4(a). (a) *Algorithm No. 1* with *h=80*, (b) *Algorithm No. 2* with *R=35,* (c) *Algorithm No. 3* with *h=80*, (d) *HPF* with window size equal to *3*, (e) *HPF* with window size equal to *5*, (f) *SLCE* with window size equal to *3.*

When observing Figures 11 and 12, one can see that the *SLCE* did not produce good results, because the *S-spikes* were not well discriminated. The *SLCE,* even if one works locally, caused an over-saturation. The obtained results when working with the *HPF* was a little better, where the *S-spikes* were more highlighted, but the background was not completely dark, and one did not achieve a good contrast in relation to the *S-proteins.* However, our *Algorithms* (especially *No. 3*) accentuated and isolated the *S-spikes*, reaching a background practically equal zero, which offered visually a better contrast.

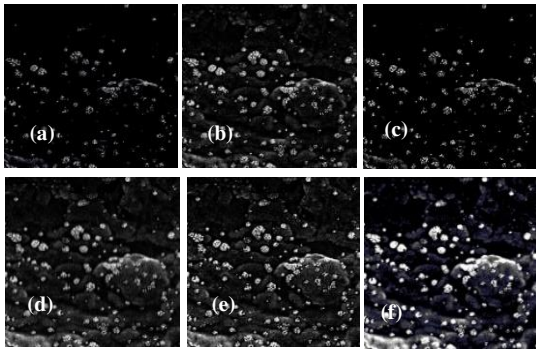

Fig. 12. Comparisons with two classical methods. Original image Fig. 5(a). (a) *Algorithm No. 1* with *h=80*, (b) *Algorithm No. 2* with *R=35,* (c) *Algorithm No. 3* with *h=80*, (d) *HPF* with window size equal to *3*, (e) *HPF* with window size equal to *5*, (f) *SLCE* with window size equal to *3.*

Qualitative comparison always generates certain subjectivity. For that reason, in order to achieve a more objective criterion of the performance of the *Algorithms,* it is necessary to carry out a quantitative comparison.

A. Quantitative comparison among the Algorithms

Due to the lack of truth images, the quantitative evaluation of enhancement and segmentation techniques are difficult to achieve. According to many authors, this remains an open problem [15]. For that reason, some quantitative comparison with manual segmentation may provide a useful indication. Manual segmentation generally gives the best and most reliable results when identifying structures for a particular clinical task (in this case, the *S-spikes*).

Thus, for this comparison a virology specialist outlined the *S-spikes* from images of Figures 4(a) and 5(a), which it was an extremely tedious work. The specialist made a bank of 15 images, of which for reasons of space, we only will show two of them, and considered as trues. The background of these images are equal to zero. Figure 13 shows the images.

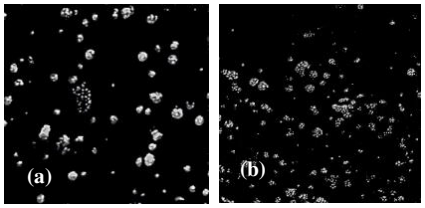

Fig. 13. Manually contrasted images from Figs 4(a) and 5(a) that we considered as trues.

Table I and Table II list the results of comparisons of manually contrasted images with those obtained by our *Algorithms*, and with the *HPF* and *SLCE*. We utilized as metrics of evaluation: *Accuracy*, *Sensitivity*, *Precision*, *Specificity* and *F-Measure* [15], [16], [17].

Table I. Comparison of manually contrasted images with those obtained by our *Algorithms*, and with the *HPF* and *SLCE.* Taking Fig. 13 (a) as *True*.

Images	*Accuracy*	*Sensitivity*	*Precision*	*Specificity*	*F-Measure*
Fig. 11 (a)	90.01	89.97	90.94	88.97	91.01
Fig. 11 (b)	87.93	87.16	86.77	86.95	84.98
Fig. 11 (c)	95.93	95.96	94.88	93.95	94.04
Fig. 11 (d)	87.03	86.89	84.13	85.03	80.90
Fig. 11 (e)	80.90	79.96	81.88	78.95	77.04
Fig. 11 (f)	70.80	72.83	60.17	71.01	68.80

Table II. Comparison of manually contrasted images with those obtained by our *Algorithms*, and with the *HPF* and *SLCE.* Taking Fig. 13 (b) as *True*.

Images	*Accuracy*	*Sensitivity*	*Precision*	*Specificity*	*F-Measure*
Fig. 12 (a)	91.01	86.97	90.94	91.97	90.01
Fig. 12 (b)	87.93	84.16	86.07	86.95	83.98
Fig. 12 (c)	96.93	95.96	94.88	95.95	96.04
Fig. 12 (d)	85.03	82.89	85.13	83.03	80.90
Fig. 12 (e)	83.90	80.96	82.88	80.95	79.04
Fig. 12 (f)	57.00	53.83	52.17	52.01	55.80

Table I and Table II reflect that the *SLCE* method was the worst of all. In all images produced an over saturation and joined the *S-spikes*, which it is manifested in the low percents obtained in the metrics (see last rows in Tables I and II).

The *HPF* technique performed better, especially when we used a *3x3* window size (see metrics in the rows five and six), but never was superior to our *Algorithms*. One can observe in Figures 11(d) and 12(d) that the *HPF* technique sharpened the high frequencies (the *S-spikes*), but the background did not reach a value close to zero. Our *Algorithms* with the use of *h* parameter, if they achieved this (which increases the contrast with the *S-proteins*). Hence the importance of this parameter.

One can see in Tables I and II the high percents obtained in the used metrics in order to evaluate quantitatively the effectiveness of the *Algorithm No. 3* (see row 3). In particular, one can note the percents in the metrics of *Sensitivity* and *Specificity*, which many authors consider important performance measures in medical images [17]. These scores show that in all cases the *Algorithm No. 3* had good behavior in

the enhancement and sharpens of the *S-spikes*, which is in line with what one can appreciate in Figures 11(c) and 12(c).

5. Conclusions

We carried out a theoretical analysis of the proposed algorithms to the enhancement and sharpening of the SARS-CoV-2 high-resolution microscopy images. We showed that the *Algorithms* arose as result of the combination of techniques in several fields of computer vision, originating hybrid strategies with a minimum amount of parameters and elegant algorithmic simplicity. We also verified the importance of the *h* parameter to obtain a background close to zero and to increase the local contrast and sharpness of the *S-proteins*. Finally, we carried out a quantitative evaluation to achieve a more objective comparison with two recognized classical algorithms. The proposed algorithms can be applied to other types of bacteria and new viruses of high-resolution microscopy images.

References

1. Roberto Rodríguez, Brian A. Mondeja; Odalys Valdes; Sonia Resik; Ananayla Vizcaino; Emilio F. Acosta; Yorexis González; Vivian Kourí; Angelina Díaz; María G. Guzmán: "SARS-CoV-2: Enhancement and Segmentation of High-Resolution Microscopy Images. Part I", Sent to Signal, Image and Video Processing Video Processing, Springer Nature, 2020. DOI: 10.21203/rs.3.rs-65818/v1
2. Yu Chen, Qianyun Liu, and Deyin Guo: "Emerging coronaviruses: genome structure, replication, and pathogenesis", Journal of medical virology, 92 (4):418-423, 2020.
3. Catharine I Paules, Hilary D Marston, and Anthony S Fauci: "Coronavirus infections|more than just the common cold", Jama, 323 (8):707-708, 2020.
4. Anwaar Ulhaq, Asim Khan, Douglas Gomes and Manoranjan Paul: "Computer Vision for COVID-19 Control: A survey", ArXiv:2004.09420v2 [eess.IV] 5 May 2020.
5. Rodríguez, R., and Sossa, J. H.: *Mathematical Techniques for Biomedical Image Segmentation*, In R. Narayan (Ed.), Encyclopedia of Biomedical Engineering, vol. 3, pp. 64–78. Elsevier. ISBN: 9780128048290, Elsevier Inc. All rights reserved. Elsevier, Copyright © 2019.
6. Brian Mondeja, Odalys Valdes, Sonia Resik, Ananayla Vizcaino, Emilio Acosta, Adelmo Montalván, Amira Paez, Mayra Mune, Roberto Rodríguez, Juan Valdés, Guelsys Gonzalez, Daisy Sanchez, Viviana Falcón, Yorexis González, Vivian Kourí, Angelina Díaz and Maria Guzmán.: "SARS-CoV-2: High-Resolution Microscopy Study in Human Nasopharyngeal Samples", sent to Virology Journal, 2020. DOI: 10.21203/rs.3.rs-36154/v1
7. https://www.who.int/emergencies/diseases/novel-coronavirus-2019
8. Rodríguez, R., Garcés, Y., Torres, E., Sossa, H. and Tovar, R.: "A vision from a physical point of view and the information theory on the image segmentation", Journal of Intelligent & Fuzzy Systems, vol. 37, pp. 2835-2845, IOS Press, 2019. DOI: 10.3233/JIFS-190030
9. Roberto Rodríguez and Juan H. Sossa, (In Spanish), Procesamiento y Análisis Digital de Imágenes, Book Published by "Ra-Ma®" Editorial, ISBN: 978-84-9964-007-8, Printed in Spain, May 2011. http://www.ra-ma.es/busqueda/listaLibros.php?tipoBus=autor&palabrasBusqueda=Roberto+Rodriguez%2C+Juan+H.+Sossa
10. Roberto Rodríguez: "A Strategy for blood vessels segmentation based on the threshold which combines statistical and scale space filter. Application to the study of angiogenesis", Journal of Computer Methods and Programs in Biomedicine (Elsevier), Vol. 82, Issue, pp. 1-9, 2006.
11. Kaiming He, Xiangyu Zhang, Shaoqing Ren, and Jian Sun: "Spatial Pyramid Pooling in Deep Convolutional Networks for Visual Recognition", D. Fleet et al. (Eds.): ECCV 2014, Part III, LNCS 8691, pp. 346–361, 2014, Springer International Publishing Switzerland 2014.
12. Anwaar Ulhaq, Asim Khan, Douglas Gomes and Manoranjan Paul: "Computer Vision for COVID-19 Control: A survey", ArXiv:2004.09420v2 [eess.IV] 5 May 2020.
13. Qingsen Yan, Bo Wang, Dong Gong, Chuan Luo, Wei Zhao, Jianhu Shen, Qinfeng Shi, Shuo Jin, Liang Zhang and Zheng You: "COVID-19 Chest CT Image Segmentation: A Deep Convolutional Neural Network Solution", ArXiv:2004.10987v2 [eess.IV] 26 Apr 2020.
14. Chaki, N., Saeed, K. and Shaikh, S. H.: Exploring Image Binarization Techniques, Studies in Computational Intelligence 560, DOI: 10.1007/978-81-322-1907, ©Springer India 2014
15. P. L. Muñoz, R. Rodríguez and N. Montalvo: "Automatic Segmentation of Diabetic foot ulcer from Mask Region-Based Convolutional Neural Networks", Journal of Biomedical Research and Clinical Investigation, Volume 1, Issue 1.1006, August 2020. DOI: https://doi.org/10.31546/2633-8653.1006
16. M. Goyal, N. D. Reeves, S. Rajbhandari, N. Ahmad, C. Wang and M. Hoon Yap, "Recognition of Ischaemia and Infection in Diabetic Foot Ulcers: Dataset and Techniques", ArXiv: 1908.05317v1 [eess.IV], Aug 2019. https://www.researchgate.net/publication/335201111

Figures

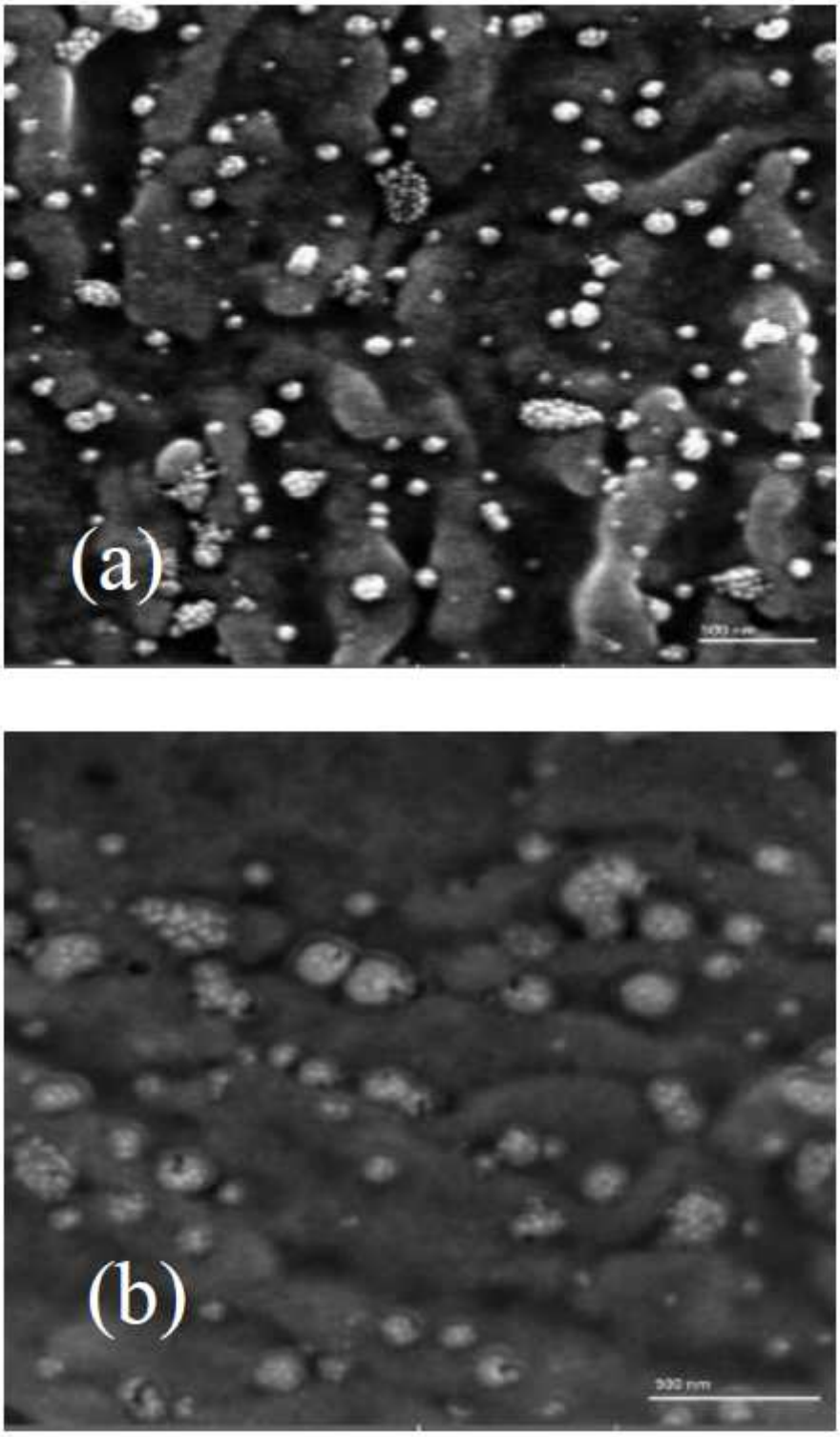

Figure 1

Characteristic of coronavirus microscopic images. (a) and (b), original microscopic images.

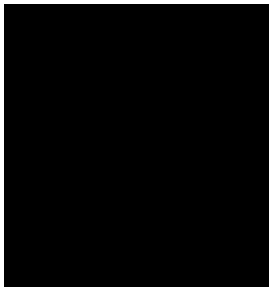

Figure 2

Figure 2 not provided in this version.

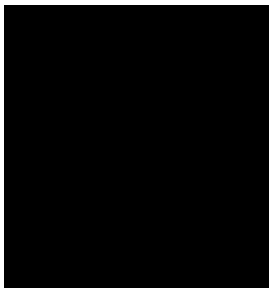

Figure 3

Figure 3 not provided in this version.

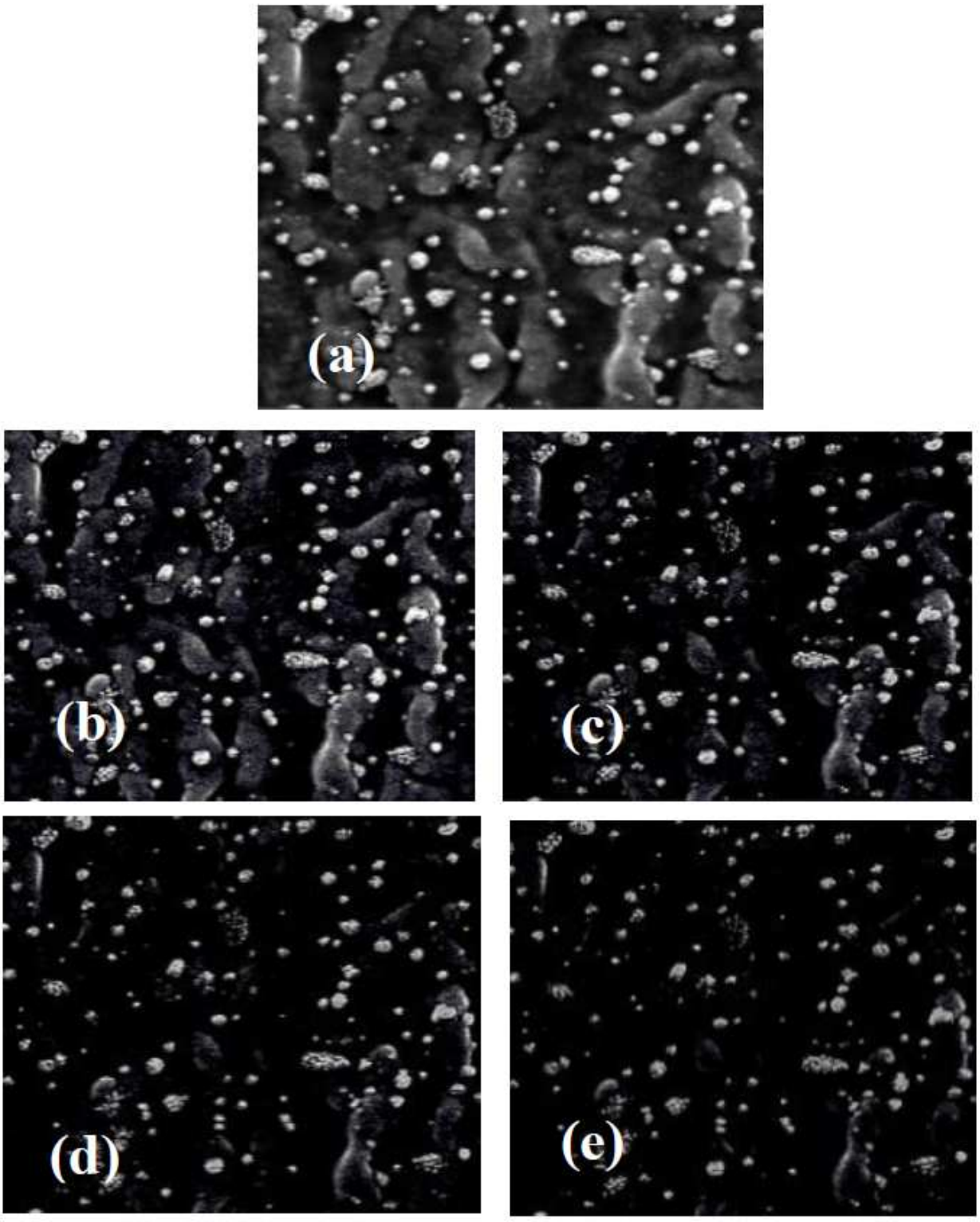

Figure 4

Application of Algorithm No. 1 for different values of h parameter. (a) Original image, (b) h=30, (c) h=60, (d) h=80, (e) h=100.

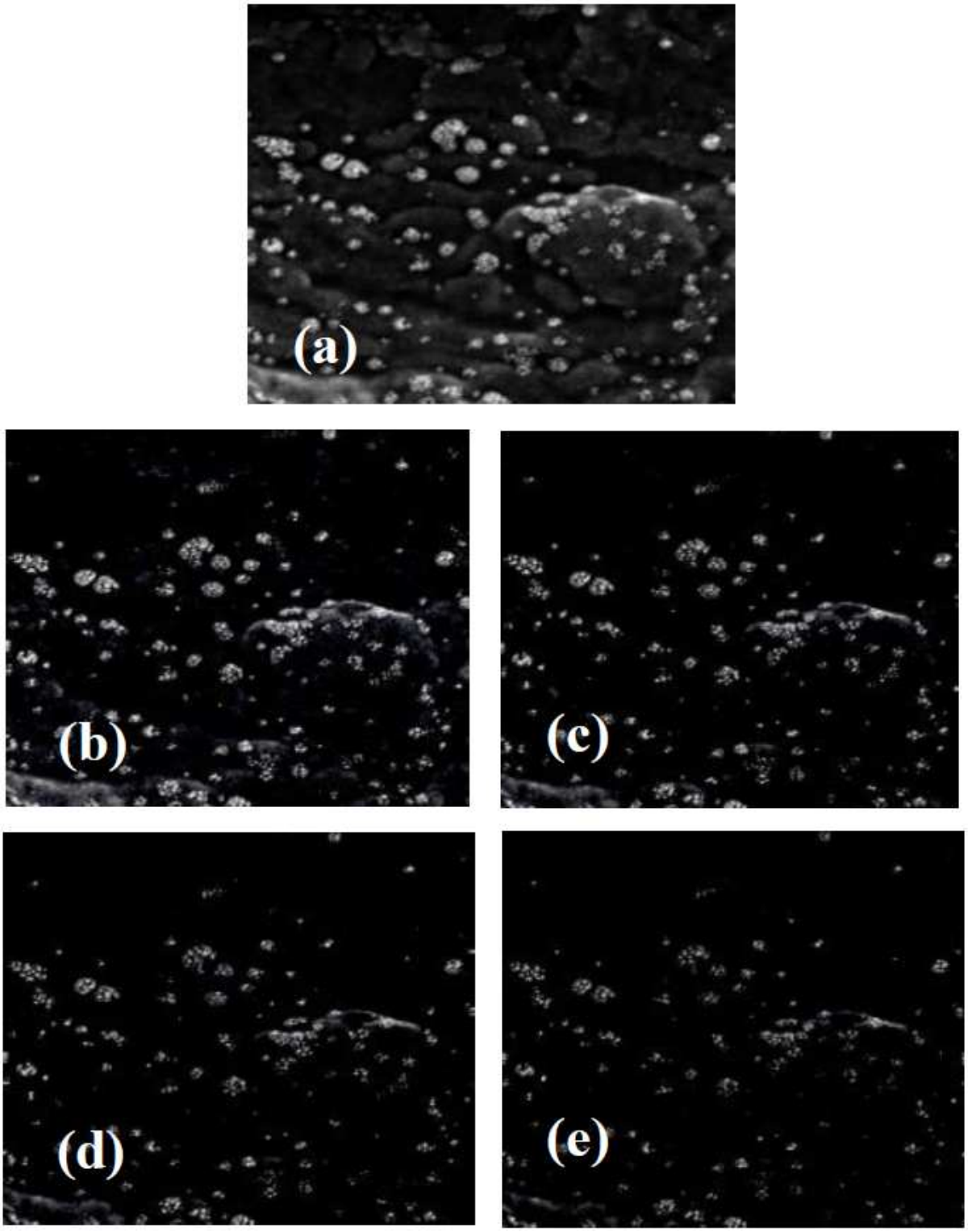

Figure 5

Application of Algorithm No. 1 for different values of h parameter. (a) Original image, (b) h=30, (c) h=60, (d) h=80, (e) h=100.

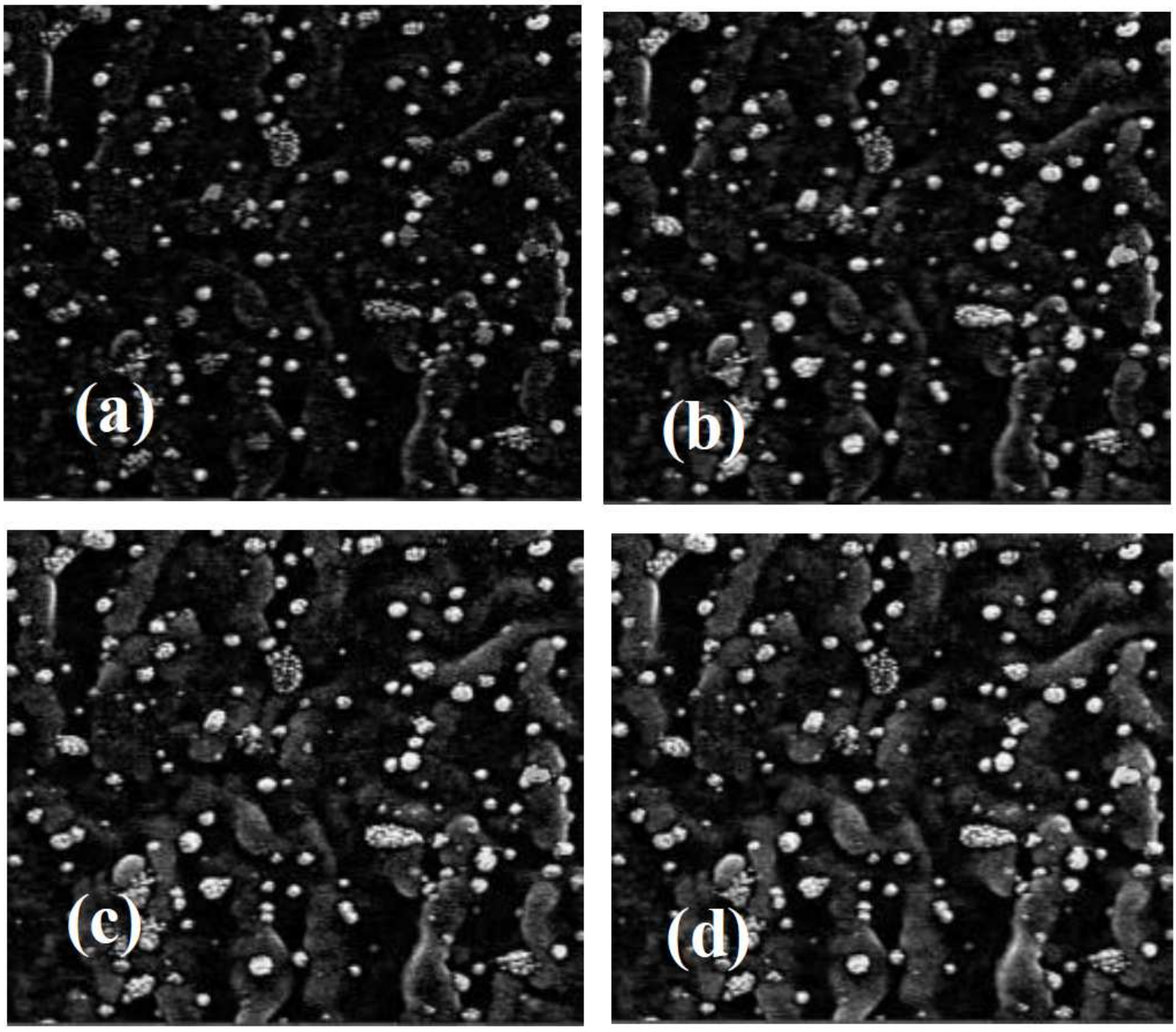

Figure 6

Application of the Algorithm No. 2 for a structuring element type “Disk” for different radios. Original image Fig. 4(a). (a) Radio =15, (b) Radio = 25, (c) Radio = 35, (d) Radio = 45.

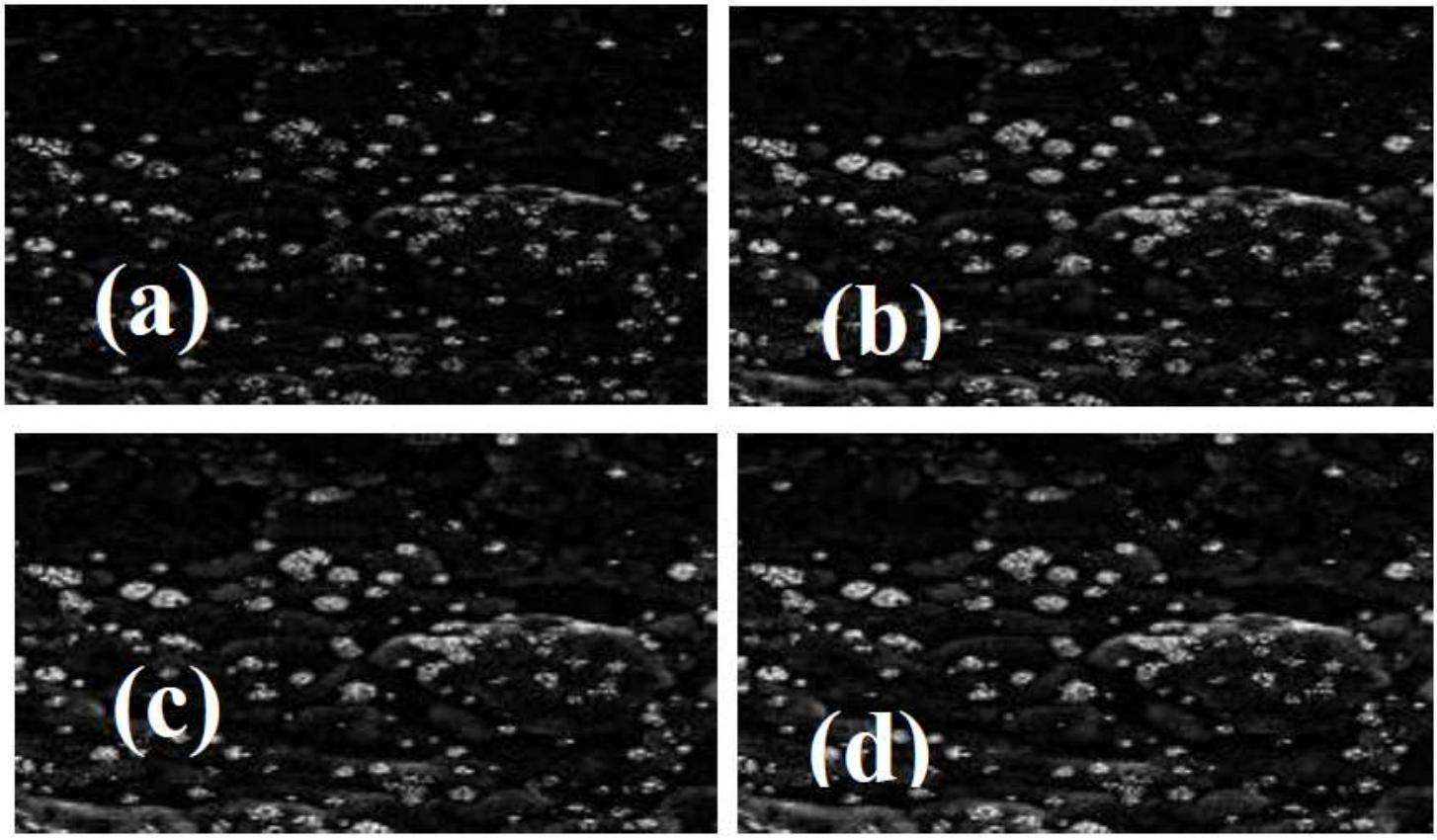

Figure 7

Application of the Algorithm No. 2 for a structuring element type “Disk” for different radios. Original image Fig. 5(a). (a) Radio =15, (b) Radio = 25, (c) Radio = 35, (d) Radio = 45.

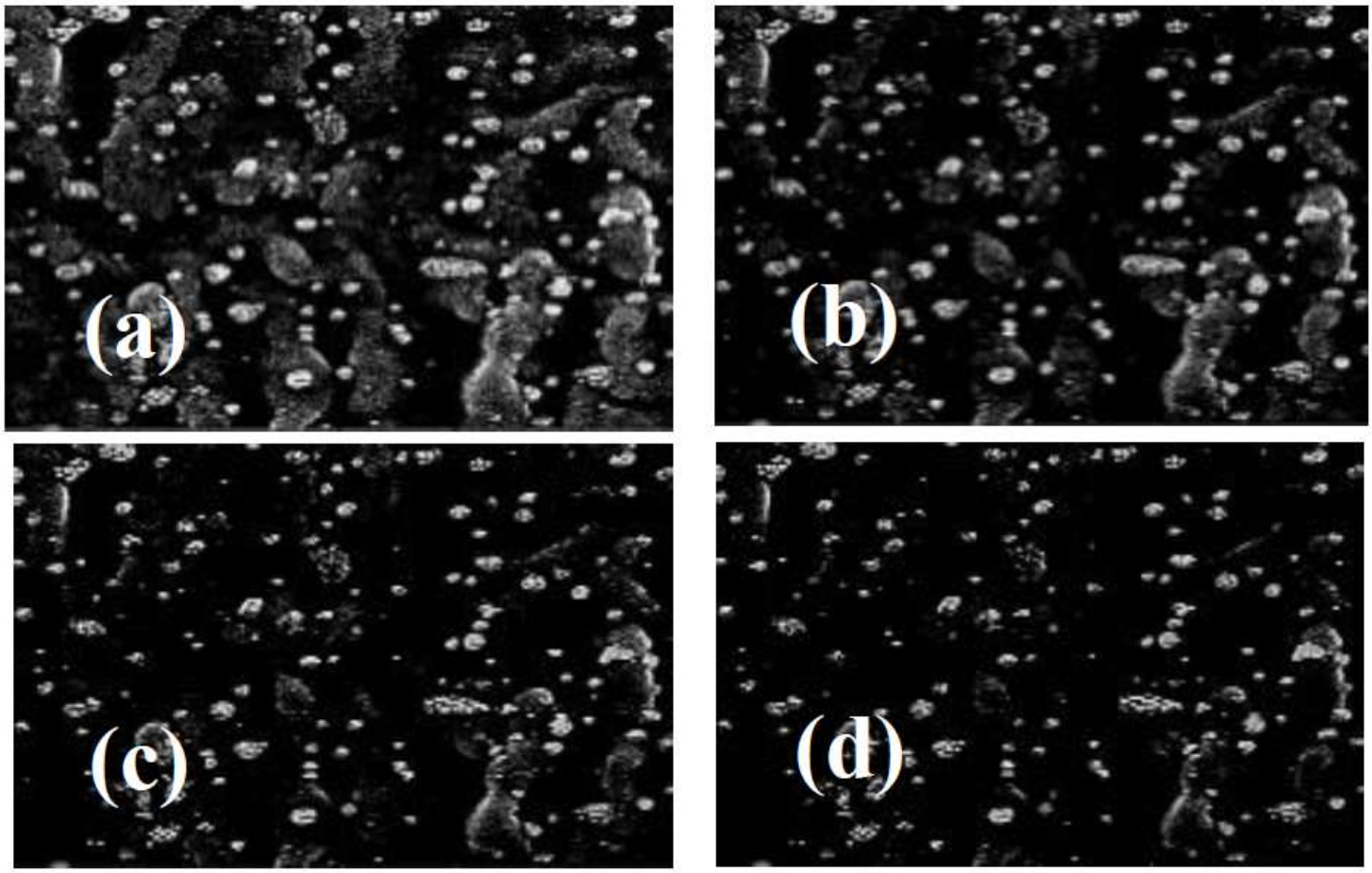

Figure 8

Application of Algorithm No. 3 for different values of h parameter. Original image Fig. 4(a). (a) h=30, (b) h=60, (c) h=80, (d) h=100.

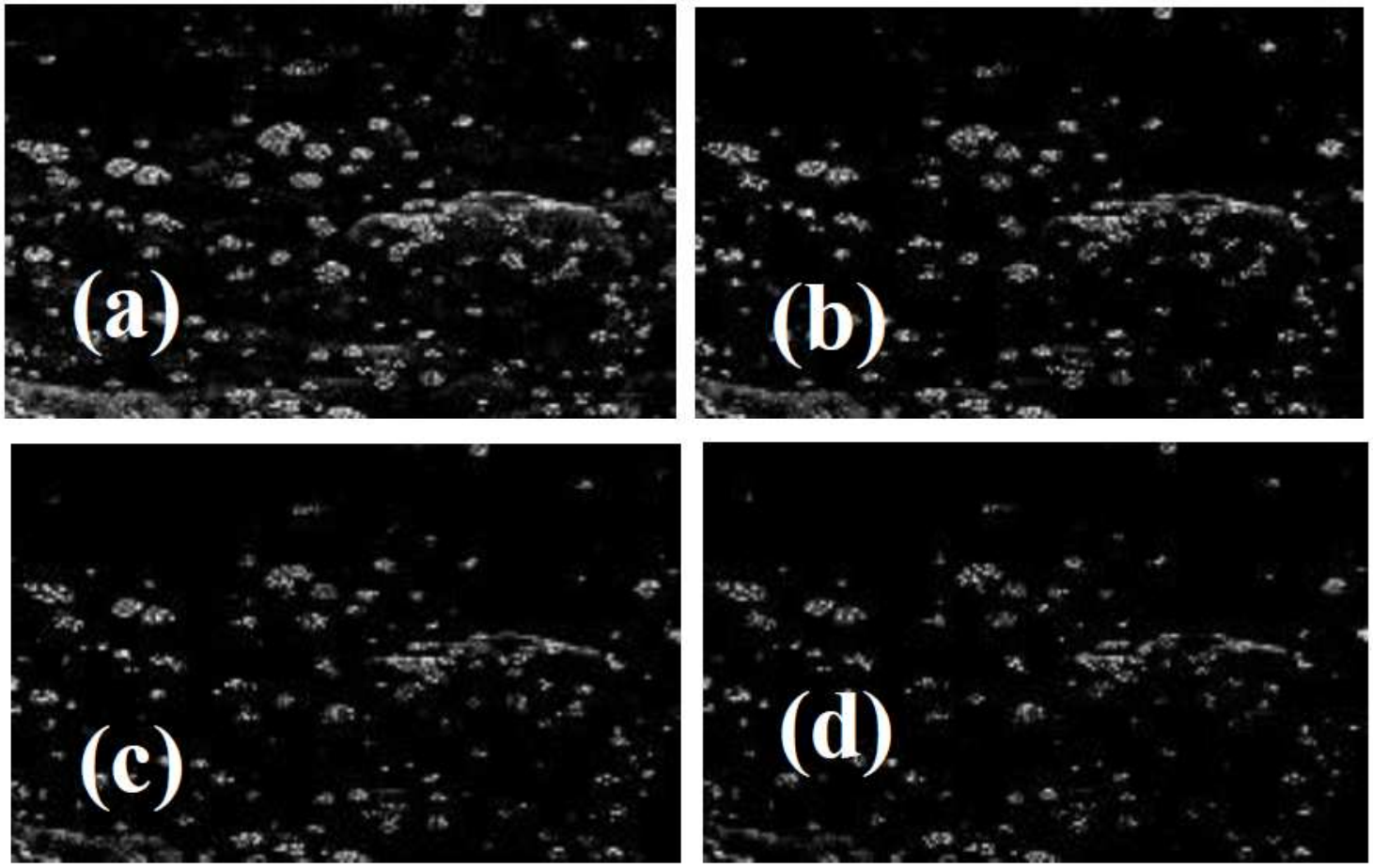

Figure 9

Application of Algorithm No. 3 for different values of h parameter. Original image Fig. 5(a). (a) h=30, (b) h=60, (c) h=80, (d) h=100.

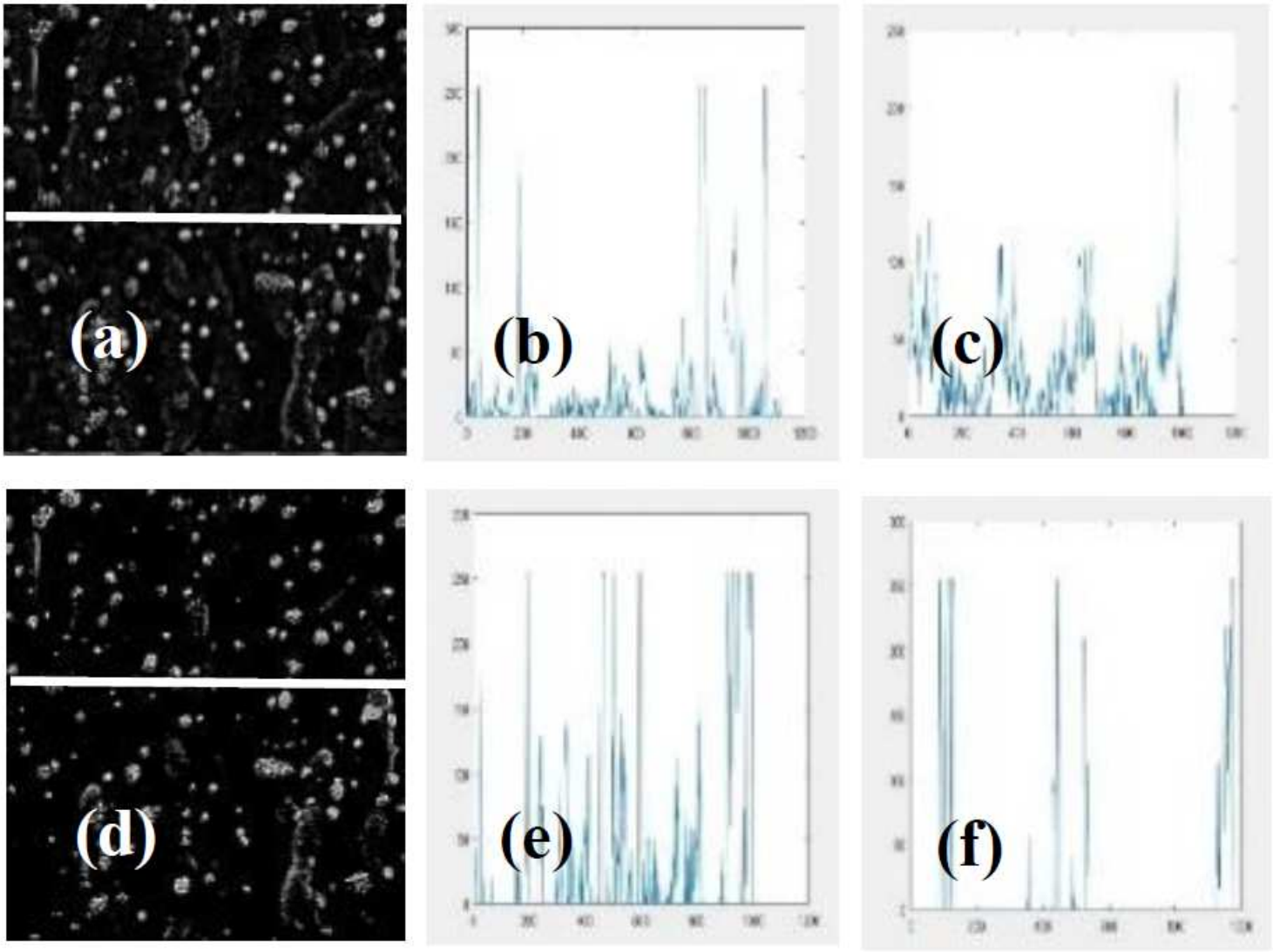

Figure 10

Profiles with the processed images by using the Algorithms No. 2 and No. 3. (a) Processed image and a profile, (b) R=15, (c) R=45, (d) Processed image and a profile, (e) h = 30, (f) h = 100.

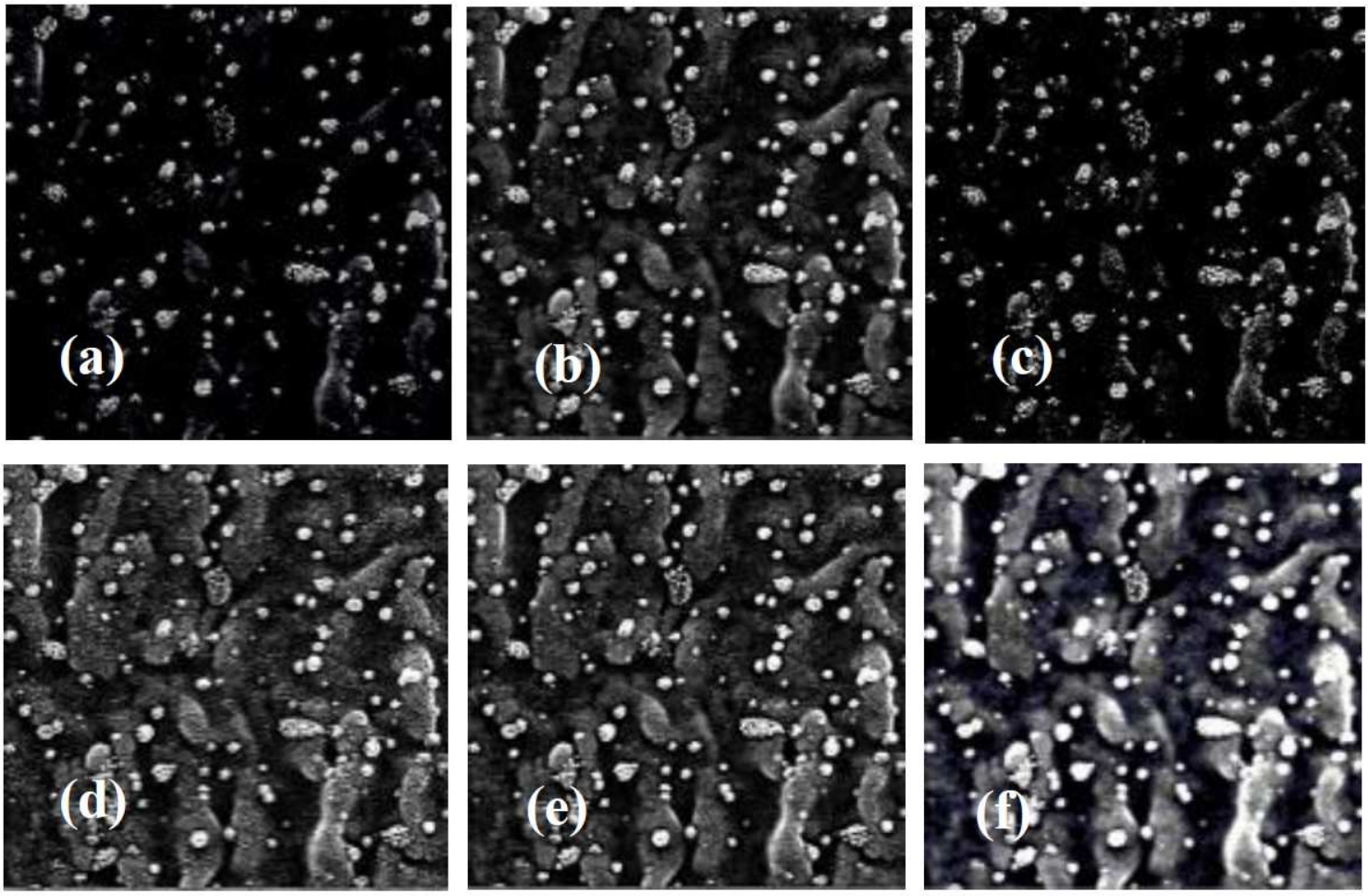

Figure 11

Comparisons with two classical methods. Original image Fig. 4(a). (a) Algorithm No. 1 with h=80, (b) Algorithm No. 2 with R=35, (c) Algorithm No. 3 with h=80, (d) HPF with window size equal to 3, (e) HPF with window size equal to 5, (f) SLCE with window size equal to 3.

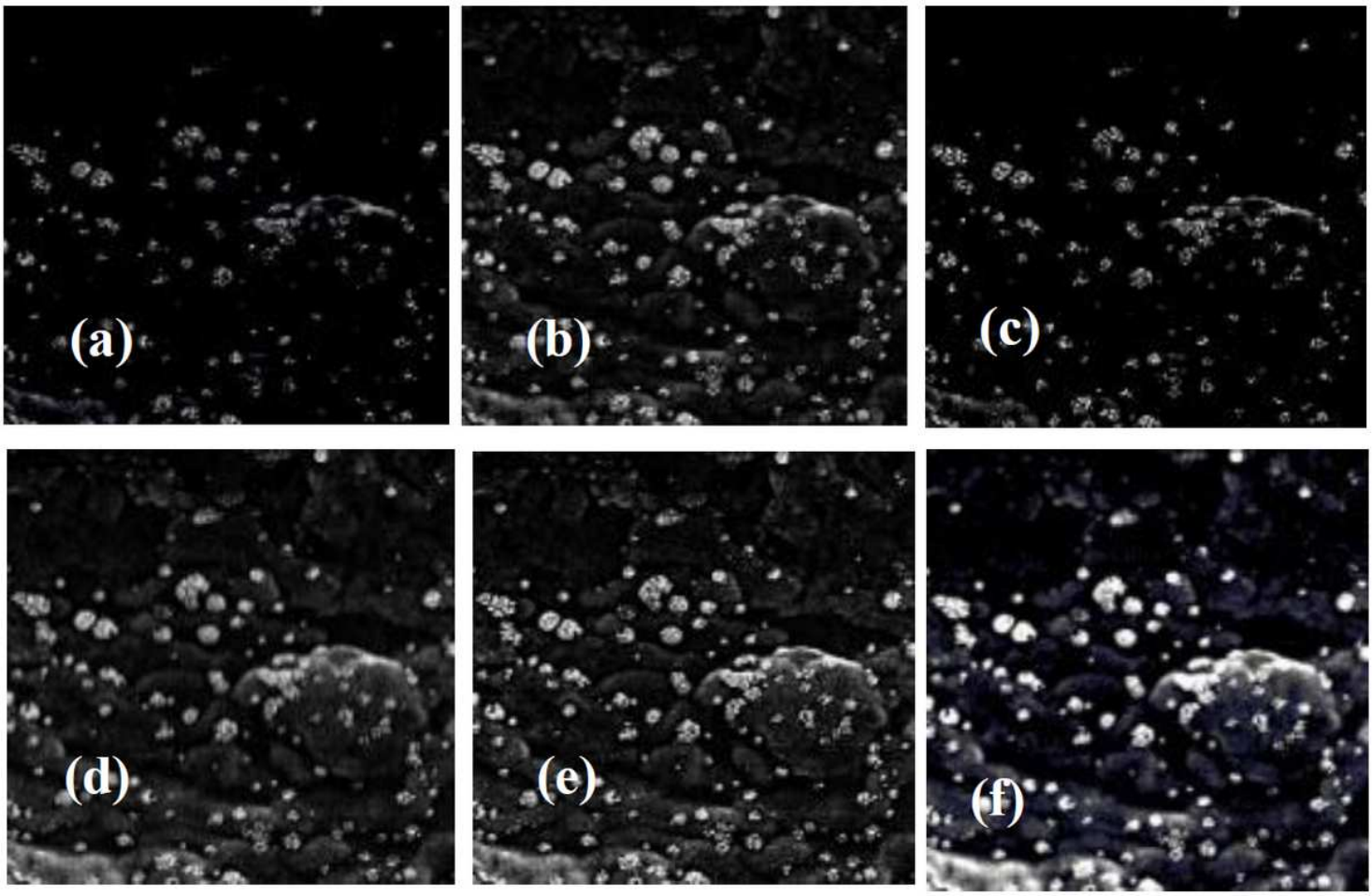

Figure 12

Comparisons with two classical methods. Original image Fig. 5(a). (a) Algorithm No. 1 with h=80, (b) Algorithm No. 2 with R=35, (c) Algorithm No. 3 with h=80, (d) HPF with window size equal to 3, (e) HPF with window size equal to 5, (f) SLCE with window size equal to 3.

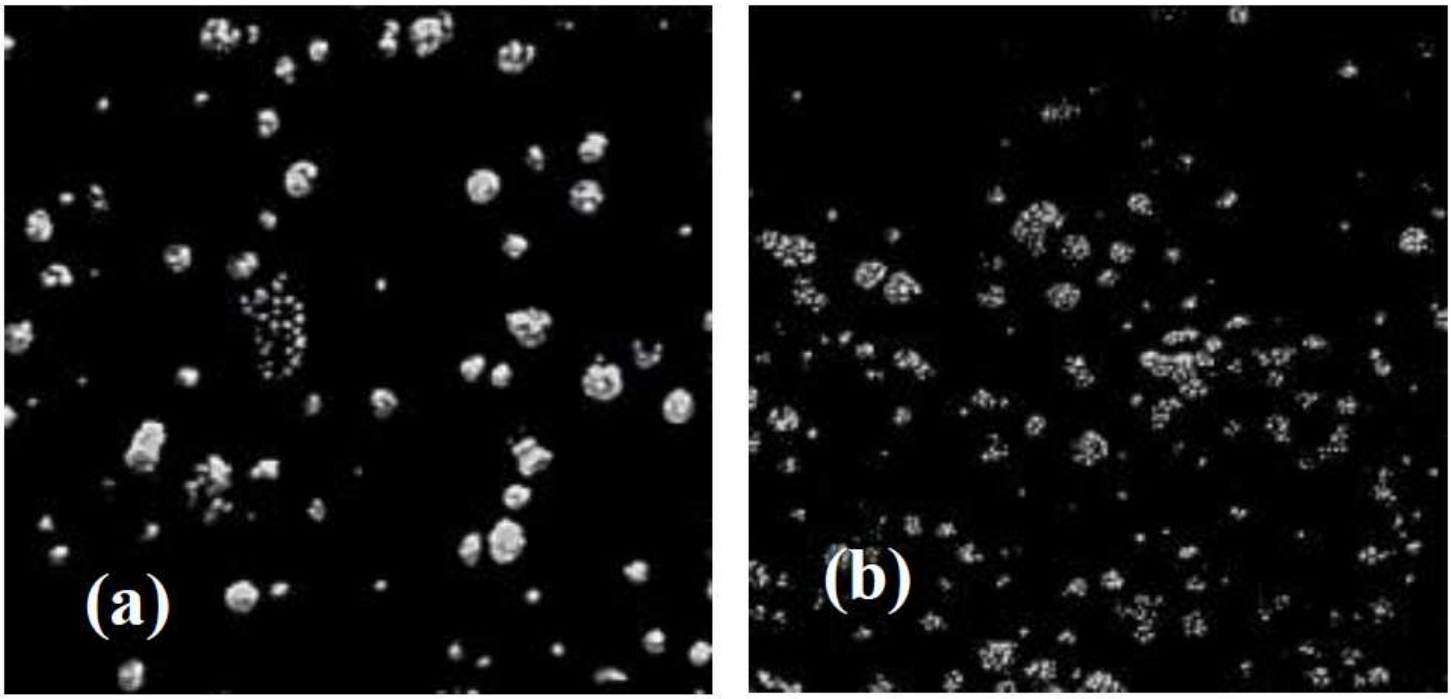

Figure 13

Manually contrasted images from Figs 4(a) and 5(a) that we considered as trues.